Schweizerischer Erdbebendienst
Service Sismologique Suisse
Servizio Sismico Svizzero
Servizi da Terratrembels Svizzer

ETH
Eidgenössische Technische Hochschule Zürich
Swiss Federal Institute of Technology Zurich

St Niklaus - Bahnhofplatz (SNIB)

SITE CHARACTERIZATION REPORT

Jan BURJANEK, Clotaire MICHEL, Gabriela GASSNER-STAMM

Valerio POGGI, Daniel ROTEN, Carlo CAUZZI, Donat FÄH

Sonneggstrasse 5 CH-8092 Zürich Switzerland; E-mail: clotaire.michel@sed.ethz.ch

Last modified : November 1, 2013

Abstract

In the narrow valley of the Mattervispa in St Niklaus was installed the new station SNIB of the Swiss Strong Motion Network. In order to characterize the velocity profile under the station, an array measurement of $240\,\mathrm{m}$ aperture performed in the frame of the COGEAR project was used. The measurements were successful in deriving a velocity model for this site. Shear wave velocities are about $500\,\mathrm{m/s}$ in the uppermost layers, with a slightly increasing value with depth. A strong velocity contrast is present at the depths of $50 - 75\,\mathrm{m}$ with velocities of $1.3\,\mathrm{Hz}$ the lower layer between 1000 and $2000\,\mathrm{m/s}$. The bedrock is probably located below this depth, but a 2D resonance with a fundamental frequency of does not allow to determine it from the ellipticity curve. $V_{s,30}$ is found to be close to $500\,\mathrm{m/s}$. The EC8 and SIA261 ground types are B. Recordings on the new station will allow to validate the proposed 1D models.

Contents

1 Introduction

The station SNIB (St Niklaus Bahnhofplatz) is part of the Swiss Strong Motion Network (SSMNet) in the Valais region (Fig. 1). SNIB was newly installed in the framework of the SSMNet Renewal project in 2010, densifying the SSMNet in the Valais in coordination with the COGEAR project. The SSMNet renewal project includes also the site characterization. The passive array measurement has been selected as a standard tool to investigate these sites. Several measurement campaigns were performed in St Niklaus in the frame of the COGEAR project. In winter 07/08 and 08/09 one of the temporary stations (STNI1) was installed in the cellar of a house close to SNIB. The most relevant measurement campaign was performed on July 24th 2006, with a centre about 40 m away from the station SNIB, in order to characterize the sediments at this site. The station is located in a narrow (250 m) alpine valley on a small sedimentary basin. This report presents the measurement setup, the results of the array processing of the surface waves (dispersion curves). Then, an inversion of these results for a velocity profile is performed.

Canton	City	Location	Station code	Site type	Slope
Valais	St Niklaus	Bahnhofplatz	SNIB	Narrow alpine valley	Slight Slope

Table 1: Main characteristics of the study-site.

Figure 1: Picture of the site.

2 Experiment description

2.1 Ambient Vibrations

The ground surface is permanently subjected to ambient vibrations due to:

- natural sources (ocean and large-scale atmospheric phenomena) below $1\,\mathrm{Hz}$,
- local meteorological conditions (wind and rain) at frequencies around $1\,\mathrm{Hz}$,
- human activities (industrial machines, traffic…) at frequencies above $1\,\mathrm{Hz}$ [Bonnefoy-Claudet et al., 2006].

The objective of the measurements is to record these ambient vibrations and to use their propagation properties to infer the underground structure. First, the polarization of the recorded waves (H/V ratio) are used to derive the resonance frequencies of the ground layers. Second, the phase delays between stations are used to derive the velocity of surface waves at different frequencies (dispersion). The information (H/V, dispersion curves) is then used to derive the properties of the soil layers using an inversion process.

2.2 Equipment

For these measurements 5 Quanterra Q330 (named NR1 to NR5) and 4 Nanometrics Taurus (named 136, 311, 312 and MFSFT) dataloggers and 9 Lennartz 3C 5 s seismometers were available (see Tab. 2). Channels names are EH1, EH2, EH3 (Q330) and HGZ, HGN, and HGE (Taurus) for Z, N, E directions, respectively. The time synchronization was ensured by GPS. The sensor are placed on a metal tripod mainly on the asphalt.

Digitizer	**Model**	**Number**	**Resolution**
	Quanterra Q330	5	$24\,\mathrm{bits}$
	Nanometrics Taurus	4	$24\,\mathrm{bits}$
Sensor type	**Model**	**Number**	**Cut-off frequency**
Velocimeter	Lennartz 3C	9	$0.2\,\mathrm{Hz}$

Table 2: Equipment used.

2.3 Geometry of the arrays

Three array configurations were used, for a total of 5 rings of 10, 25, 40, 70 and $120\,\mathrm{m}$ radius around a central station. The first configuration includes the 2 inner rings with 9 sensors; the second configuration includes the third and fourth rings with 9 sensors and the third configuration includes the outer ring with 9 sensors. The minimum inter-station distance and the aperture are therefore 10 and $240\,\mathrm{m}$, respectively. The experimental setup is displayed in Fig. 2. The final usable datasets are detailed in section 3.2.

Figure 2: Geometry of the arrays.

2.4 Positioning of the stations

The sensor coordinates were measured using a theodolite for the inner rings and a classical GPS device for the largest ring (c3).

3 Data quality

3.1 Usable data

The largest time windows were extracted, for which most of the sensors of the array were in position and the GPS synchronization was ensured. The characteristics of the datasets are detailed in Tab. 3. For dataset 2, station NR2 was synchronized only during $32\,\mathrm{min}$, for dataset 3, station NR5 was synchronized only from 15:30 on and station NR3 was synchronized only during $49\,\mathrm{min}$.

3.2 Data processing

The data were first converted to SAC format including in the header the sensor coordinates (CH1903 system), the recording component and a name related to the position. The name starts with ST1R, then 1 number for the configuration, _R and 1 number for the position in the configuration. Recordings were not corrected from the instrument response, involving a systematic difference in amplitude between the Q330 and the Taurus stations of about 5%.

Dataset	**Starting Date**	**Time**	**Length**	F_s	**Min. inter-distance**	**Aperture**	**# of points**
ST1R1	2006/07/24	10:22	72 min	200 Hz	10 m	50 m	9
ST1R2	2006/07/24	12:26	68 min	200 Hz	40 m	140 m	9
ST1R3	2006/07/24	14:58	73 min	200 Hz	60 m	240 m	9

Table 3: Usable datasets.

4 Array processing

4.1 Methods

The first array method we used is based on the high-resolution beam-forming (HRBF). It was originally proposed by Capon [1969] but developed and applied to vertical recordings of ambient vibrations by Kind et al. [2005]. We have extended this method to analyze also the horizontal components [Fäh et al., 2008]. Ambient noise consists mostly of surface-waves, and surface-waves are behaving dispersive. This means that wave-packages with different frequency content are propagating with different velocities. In general, subarrays with different apertures are set up for the measurement to optimize the resolution in a certain frequency band. Small apertures are used to resolve the shallow part of a structure, and by increasing the aperture, deeper and deeper structures can be investigated. The final dispersion curve over a wide frequency range is then composed of the parts obtained by the different subarrays. The limits of each subarray are given by the aliasing at high frequencies and the loss of resolution at low frequencies.

Ellipticity of Rayleigh waves was shown to be useful additional constrain for the inversion of dispersion curves [Fäh et al., 2003]. The estimate of ellipticity by f-k method (array method) was introduced by Poggi and Fäh [2010]. It is based on the assumption that a peak in the f-k cross-spectrum obtained from horizontal (radial-polarized) and vertical components of motion must be representative of the signal power of a particular Rayleigh wave mode. Thus the relative frequency-dependent surface displacement ratio can be calculated for each mode separately, once the mode-correspondent dispersion curve is identified on the f-k plane.

In the wavelet-based method of ellipticity estimation, the time-frequency representations of the vertical and both horizontal components are computed using continuous wavelet transform (CWT). In contrast to Love waves, Rayleigh waves will have an energy maximum on the vertical component. Therefore, to extract mostly Rayleigh waves, the absolute value of the CWT for the vertical component is scanned for all maxima. For each maximum identified on the time axis, the value of horizontal component wavelet coefficient is picked with a delay of one quarter of period. That is the theoretical delay between vertical and horizontal components for a Rayleigh wave. It can be positive (prograde particle motion) or negative (retrograde particle motion). The ratio between horizontal and vertical values is saved for each maximum found on the vertical component. Ratios are analyzed statistically, and the whole process is repeated for all frequencies, so the ellipticity of fundamental Rayleigh wave is estimated. We apply a method that was developed during the European project NERIES (Network of Research Infrastructures for European Seismology) joint research activity JRA4 [Fäh et al., 2009].

4.2 Results

Recordings were processed by different high-resolution FK methods. It was possible to follow the dispersion curve of fundamental mode of both Rayleigh and Love wave down to 2Hz with FK method. All picked dispersion curves for both Love and Rayleigh waves are plotted in Fig. 3. Note the remarkable agreement between different codes and methods.

Ellipticity of Rayleigh waves was estimated using wavelet-based (TFA) method and FK method. All ellipticity curves are depicted in Fig. 4. The scatter between curves retrieved by

TFA method is high from station to station. The mean TFA curve is in good agreement with FK curve.

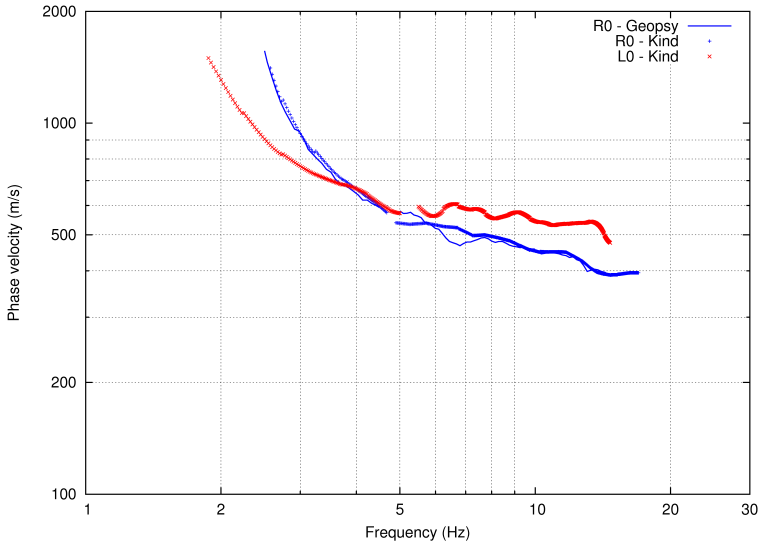

Figure 3: Dispersion curves for StN_Array1 array: R0 stands for fundamental mode of Rayleigh waves, L0 stands for fundamental mode of Love waves.

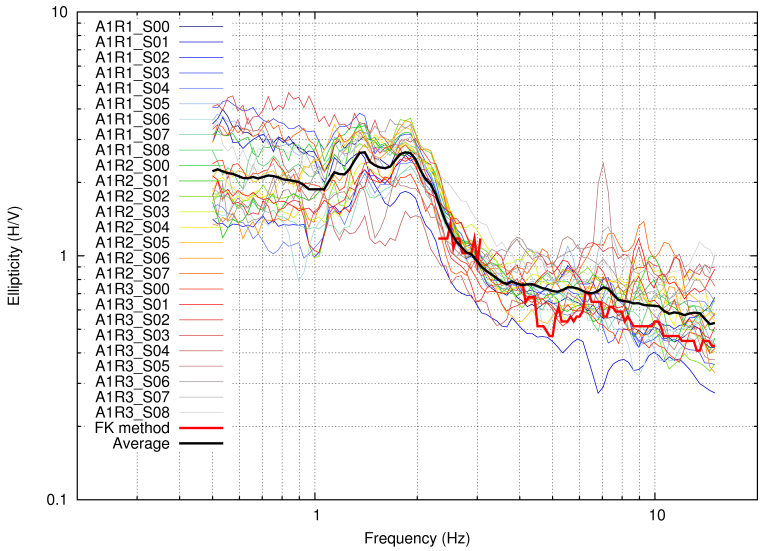

Figure 4: Ellipticity curves for StN_Array1 array obtained by wavelet and FK method.

5 Inversion and interpretation

5.1 Inversion

For the inversion we used "dinver", implemented within the GEOPSY software package (`http://www.geopsy.org`). Dinver is using the Conditional Neighbourhood Algorithm for solving inversion problems [Wathelet, 2008].

Models are parametrized by 15 layers of fixed thickness and a density of 2100kg/m3 was used for the final inversion. As 2D resonance has been identified in the valley, there is no meaning in inverting the fundamental frequency. Inversion of the DC (fundamental for both Rayleigh and Love waves) was performed with a reasonable result (see Fig. 5 and Fig. 6). Retrieved shear wave velocity profile (Fig. 7) is reliable down to 80 m, as the scatter increases rapidly below 80 m. The bedrock depth is not very well constrained, as 2D resonance likely occurs (i.e., there is a hard bedrock, but the uncertainty in the depth is likely larger than the one observed within presented models). 40 models were selected for further elaborations (Fig. 8).

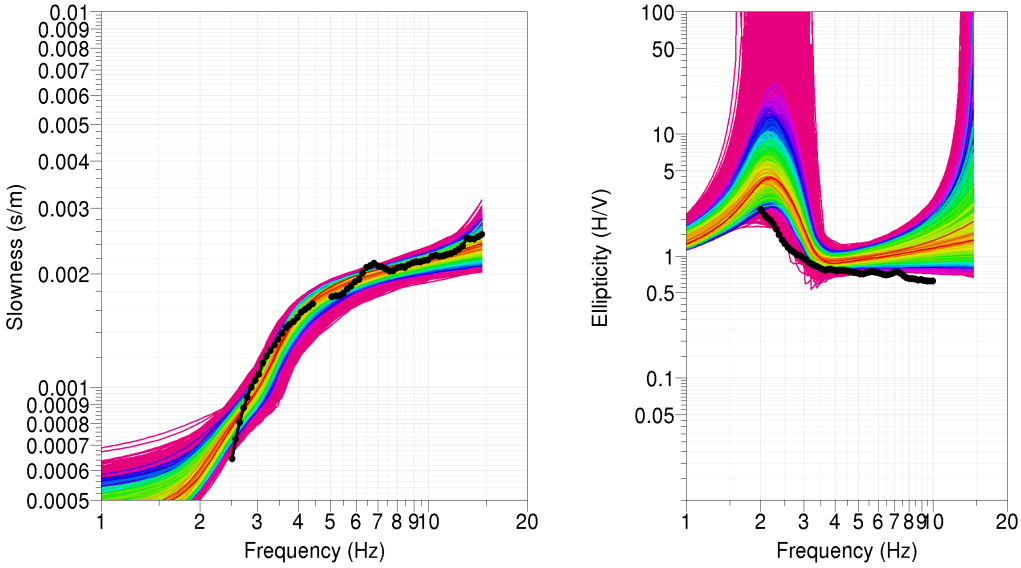

Figure 5: An ensemble of dispersion curves (left) and ellipticities (right) of fundamental mode of Rayleigh waves. Observed curves used in the inversion are in black, the color distinguishes the misfit value. Corresponding models are in the Fig. 7.

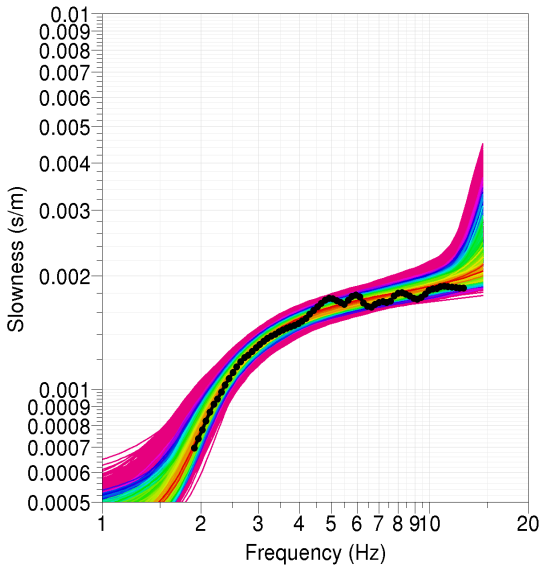

Figure 6: An ensemble of dispersion curves of the fundamental mode of Love waves. Observed curves used in the inversion are in black, the color distinguishes the misfit value. Corresponding models are in the Fig. 7.

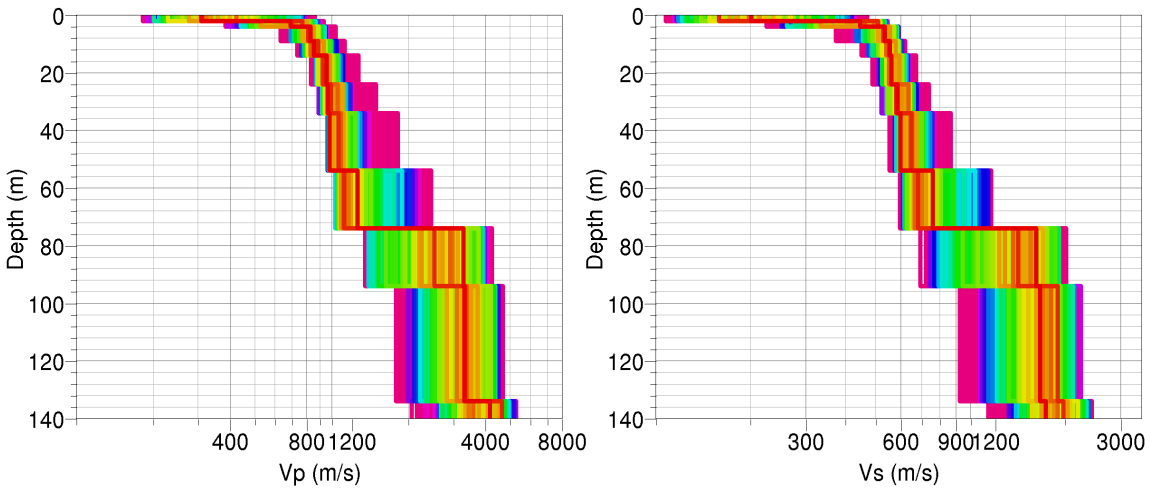

Figure 7: An ensemble of inverted velocity profiles. Colors distinguish the misfit value in the same way as in the Fig. 5 and Fig. 6.

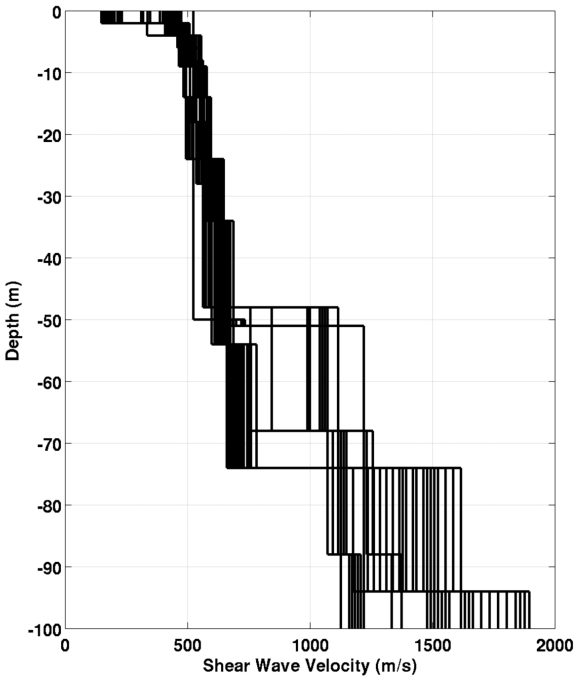

Figure 8: V_s ground profiles for the selected 40 best models.

5.2 Interpretation

Shear wave velocities are about 500 m/s in the uppermost layers, with a slightly increasing value with depth. A strong velocity contrast is present at the depths of 50 - 75 m. The next discontinuity is around a depth of 120 m. This discontinuity is probably not real, due to the 2D structure of the U-shaped valley fill. The infill is consisting mainly of alternating layers of gravel, moraine and fluvial deposits. In the frame of the COGEAR project, a student project (Eyer, 2008) estimated a cross-section of the valley from which the bedrock depth at SNIB would be between 100 and $160\,\mathrm{m}$.

A potential 2D SH resonance was identified at frequency of 1.3 Hz (Fig. 9) [Burjánek et al., 2010]. The results are consistent with the findings by Fritsche [2008]. They found at most of the locations in St Niklaus a clear polarization in the direction approximately perpendicular to the valley axis (from east to southeast). The concerning frequencies are around 1.9 Hz. This part of the wave field was interpreted as the fundamental mode of SV (SV0). On the other hand almost all locations showed a polarization along the valley axis (north-northeast). The frequencies varied in the range of 1.3 to 1.4 Hz. Accordingly to the direction of the polarization this part of the wave field was identified as the fundamental mode of SH (SH0). These values of (SV0) ≈ 1.9 Hz and of (SH0) ≈ 1.4 Hz can be explained by theory. Thus the assumption that the Valley of Vispa is characterized by a 2-D resonance in the region of St Niklaus is probably correct.

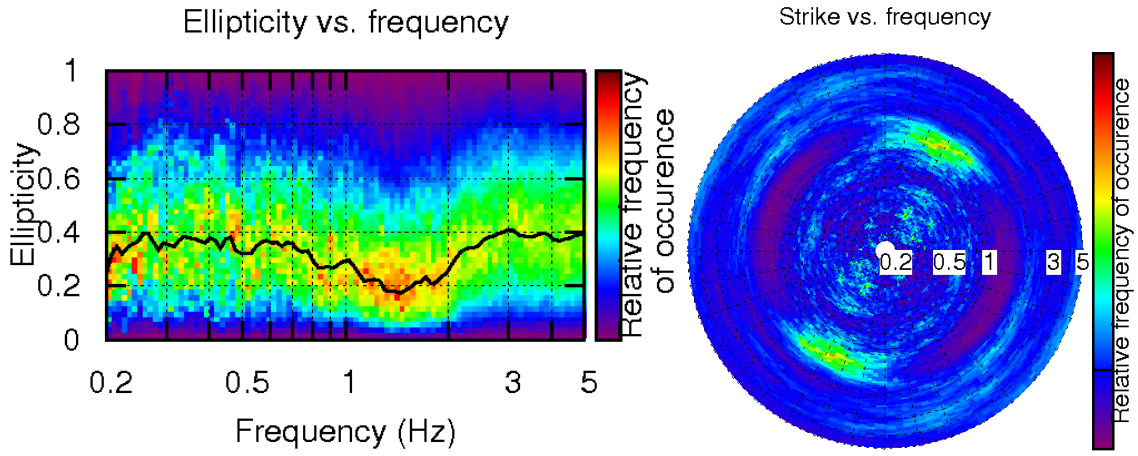

Figure 9: Polarization analysis at point R3_S06. Left: Ellipticity (A trough in the ellipticity corresponds to polarized motion). Right: Strike of the polarization.

5.3 Travel time average velocities and ground type

The distribution of the travel time average velocities at different depths was computed from the selected models. The uncertainty, computed as the standard deviation of the distribution of travel time average velocities for the considered models, is also provided, but its meaning is doubtful since the parameter space was not fully explored. $V_{s,30}$ is found to be $505\,\mathrm{m/s}$, that is associated to type B in the Eurocode 8 [CEN, 2004] and SIA261 [SIA, 2003].

	Mean (m/s)	**Uncertainty (m/s)**
$V_{s,5}$	399	97
$V_{s,10}$	443	61
$V_{s,20}$	481	30
$V_{s,30}$	505	16
$V_{s,40}$	524	11
$V_{s,50}$	540	14
$V_{s,100}$	706	20
$V_{s,150}$	-	-
$V_{s,200}$	-	-

Table 4: Travel time averages at different depths from the inverted models. Uncertainty is given as one standard deviation from the selected profiles.

5.4 SH transfer function and quarter-wavelength velocity

The quarter-wavelength velocity approach [Joyner et al., 1981] provides, for a given frequency, the average velocity at a depth corresponding to 1/4 of the wavelength of interest. It is useful to identify the frequency limits of the experimental data (minimum frequency in dispersion curves at $2\,\mathrm{Hz}$ here). The results using this proxy show that the dispersion curves constrain the profiles down to $75\,\mathrm{m}$ (Fig. 10). Moreover, the quarter wavelength impedance-contrast introduced by Poggi et al. [2012] is also displayed in the figure. It corresponds to the ratio between two quarter-wavelength average velocities, respectively from the top and the bottom part of the velocity profile, at a given frequency [Poggi et al., 2012]. It shows a trough (inverse shows a peak) at the resonance frequency.
Moreover, the theoretical SH-wave transfer function for vertical propagation [Roesset, 1970] is computed from the inverted profiles. It is compared to the quarter-wavelength amplification [Joyner et al., 1981], that however cannot take resonances into account (Fig. 11). In this case, the models are predicting an amplification of about 3 above the resonance frequency ($1.3\,\mathrm{Hz}$).

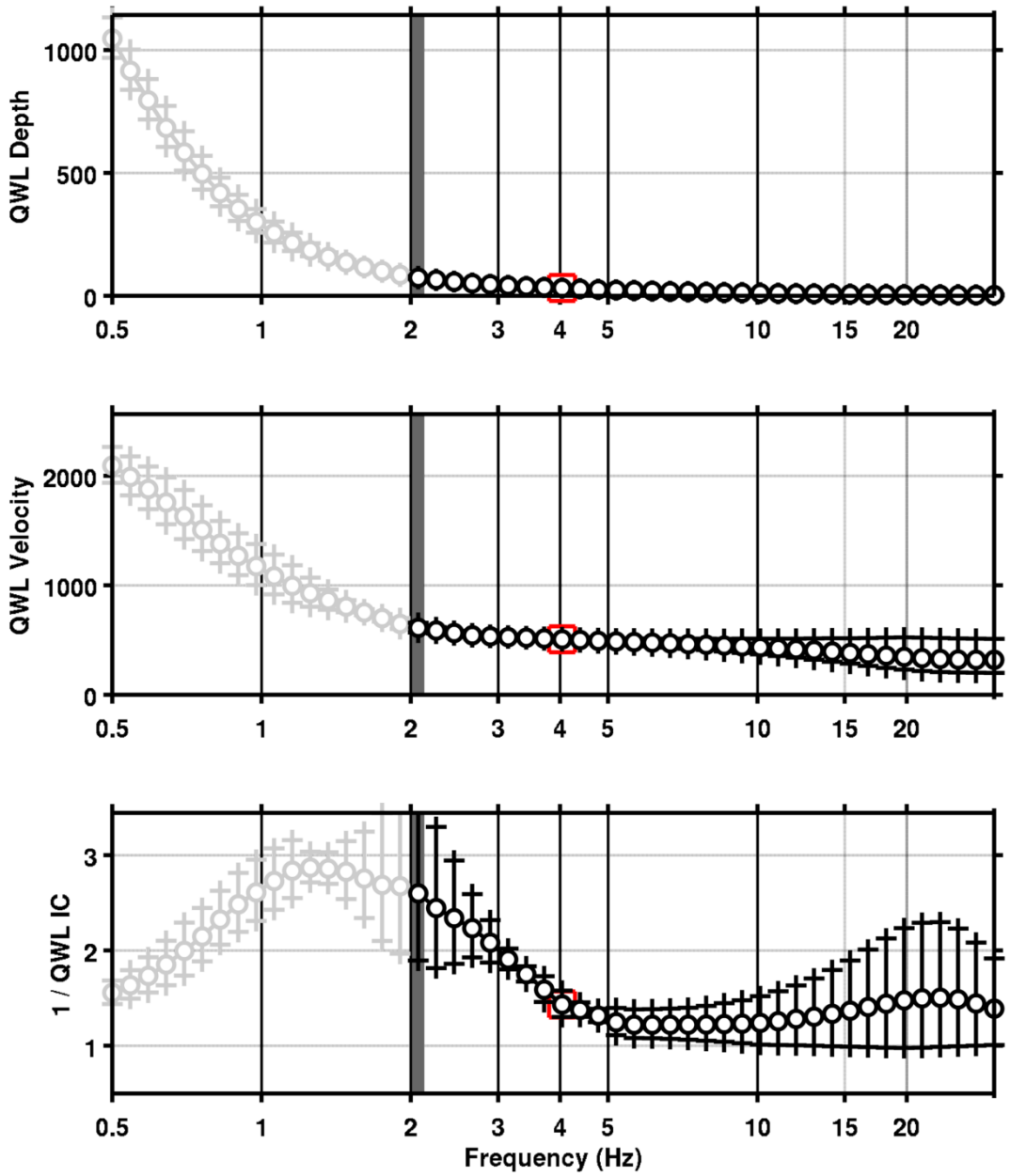

Figure 10: Quarter wavelength velocity representation of the velocity profile (top: depth, centre: velocity, bottom: inverse of the impedance contrast). Black curve is constrained by the dispersion curves, light grey is not constrained by the data. Red square is corresponding to $V_{s,30}$.

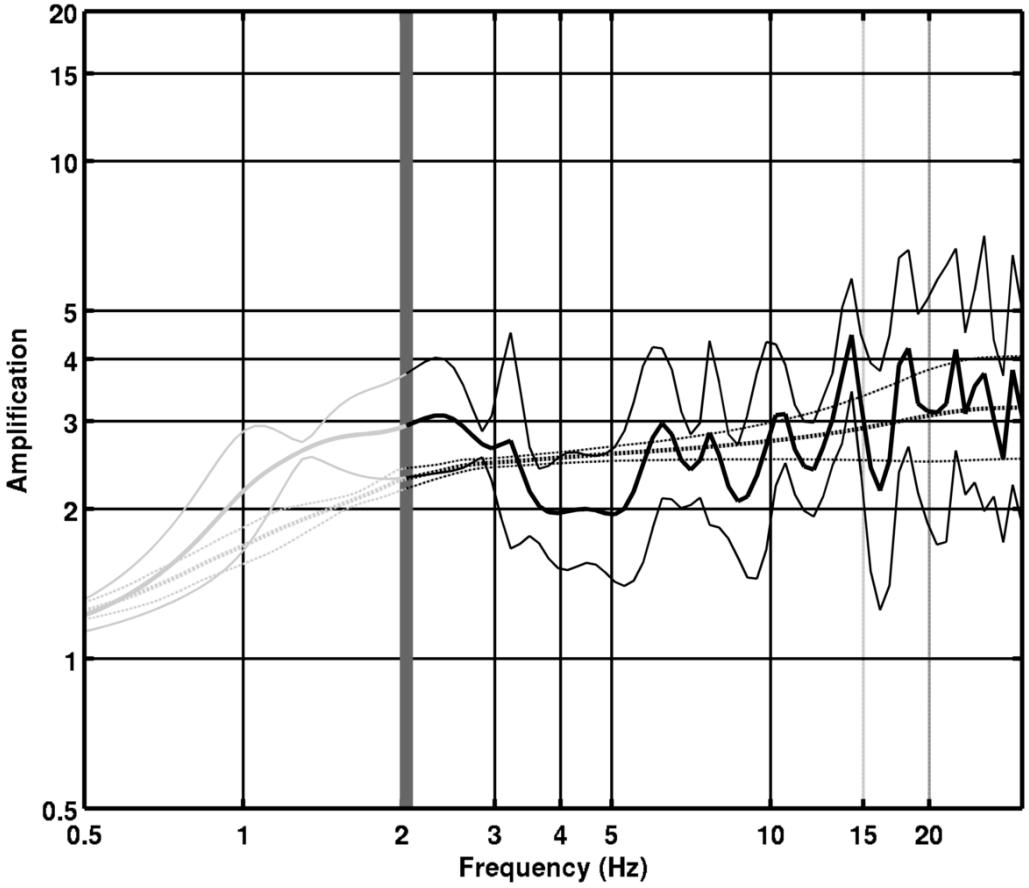

Figure 11: Theoretical SH transfer function (solid line) and quarter wavelength impedance contrast (dashed line) with their standard deviation. Significance of the greyshades is detailed in Fig. 10.

6 Conclusions

The array measurements presented in this study were successful in deriving a velocity model for the train station site in St Niklaus, below the SNIB station. Shear wave velocities are about 500 m/s in the uppermost layers, with a slightly increasing value with depth. A strong velocity contrast is present at the depths of 50 - 75 m with velocities of the lower layer between 1000 and 2000 m/s. The bedrock is probably located below this depth, but a 2D resonance does not allow to determine it from the ellipticity curve. $V_{s,30}$ is found to be close to $500\,\mathrm{m/s}$. The EC8 and SIA261 ground types are B. Recordings on the new station will allow to validate the proposed 1D models.

References

Sylvette Bonnefoy-Claudet, Fabrice Cotton, and Pierre-Yves Bard. The nature of noise wavefield and its applications for site effects studies. *Earth-Science Reviews*, 79(3-4): 205–227, December 2006. ISSN 00128252. doi: 10.1016/j.earscirev.2006.07.004. URL http://linkinghub.elsevier.com/retrieve/pii/S0012825206001012.

Jan Burjánek, Gabriela Gassner-Stamm, and Donat Fäh. COGEAR Module 3: Array measurements in the area of Visp and St. Niklaus. Technical report, Swiss Seismological Service, ETH Zürich, Zürich, 2010.

J. Capon. High-Resolution Frequency-Wavenumber Spectrum Analysis. *Proceedings of the IEEE*, 57(8):1408–1418, 1969.

CEN. *Eurocode 8: Design of structures for earthquake resistance - Part 1: General rules, seismic actions and rules for buildings*. European Committee for Standardization, en 1998-1: edition, 2004.

Donat Fäh, Fortunat Kind, and Domenico Giardini. Inversion of local S-wave velocity structures from average H/V ratios, and their use for the estimation of site-effects. *Journal of Seismology*, 7(4):449–467, October 2003. ISSN 1383-4649. doi: 10.1023/B:JOSE.0000005712.86058.42. URL http://link.springer.com/10.1023/B:JOSE.0000005712.86058.42.

Donat Fäh, Gabriela Stamm, and Hans-Balder Havenith. Analysis of three-component ambient vibration array measurements. *Geophysical Journal International*, 172(1):199–213, January 2008. ISSN 0956540X. doi: 10.1111/j.1365-246X.2007.03625.x. URL http://doi.wiley.com/10.1111/j.1365-246X.2007.03625.x.

Donat Fäh, Marc Wathelet, Miriam Kristekova, Hans-Balder Havenith, Brigitte Endrun, Gabriela Stamm, Valerio Poggi, Jan Burjanek, and Cécile Cornou. Using Ellipticity Information for Site Characterisation Using Ellipticity Information for Site Characterisation. Technical report, NERIES JRA4 Task B2, 2009.

Stefan Fritsche. *Large Historical Earthquakes in Switzerland Multidisciplinary Studies on Damage Fields and Site-Effects*. PhD thesis, ETH Zurich, 2008.

William B. Joyner, Richard E. Warrick, and Thomas E. Fumal. The effect of Quaternary alluvium on strong ground motion in the Coyote Lake, California, earthquake of 1979. *Bulletin of the Seismological Society of America*, 71(4):1333–1349, 1981.

Fortunat Kind, Donat Fäh, and Domenico Giardini. Array measurements of S-wave velocities from ambient vibrations. *Geophysical Journal International*, 160(1):114–126, December 2005. ISSN 0956540X. doi: 10.1111/j.1365-246X.2005.02331.x. URL http://gji.oxfordjournals.org/cgi/doi/10.1111/j.1365-246X.2005.02331.x.

Valerio Poggi and Donat Fäh. Estimating Rayleigh wave particle motion from three-component array analysis of ambient vibrations. *Geophysical Journal International*, 180(1):251–267, January 2010. ISSN 0956540X. doi: 10.1111/j.1365-246X.2009.04402.x. URL http://doi.wiley.com/10.1111/j.1365-246X.2009.04402.x.

Valerio Poggi, Benjamin Edwards, and Donat Fäh. Characterizing the Vertical-to-Horizontal Ratio of Ground Motion at Soft Sediment-Sites. *Bulletin of the Seismological Society of America*, 102(6), 2012. doi: 10.1785/0120120039.

J.M. Roesset. Fundamentals of soil amplification. In R. J. Hansen, editor, *Seismic Design for Nuclear Power Plants*, pages 183–244. M.I.T. Press, Cambridge, Mass., 1970. ISBN 978-0-262-08041-5. URL `http://mitpress.mit.edu/catalog/item/default.asp?ttype=2\&tid=5998`.

SIA. *SIA 261 Actions sur les structures porteuses*. Société suisse des ingénieurs et des architectes, Zürich, sia 261:20 edition, 2003.

Marc Wathelet. An improved neighborhood algorithm: Parameter conditions and dynamic scaling. *Geophysical Research Letters*, 35(9):1–5, May 2008. ISSN 0094-8276. doi: 10.1029/2008GL033256. URL `http://www.agu.org/pubs/crossref/2008/2008GL033256.shtml`.